U. S. AIR FORCE

PROJECT RAND

RESEARCH MEMORANDUM

PRELIMINARY ANALYSIS OF A SATELLITE RECOVERY SYSTEM

Richard H. Frick

RM-2264

September 19, 1958

ASTIA Document Number AD 209777

Assigned to _____

52

The RAND Corporation
1700 MAIN ST. • SANTA MONICA • CALIFORNIA

SUMMARY

This report presents a preliminary analysis of the capabilities of a satellite recovery system. In the discussion of the problem it is assumed that at some point of a satellite orbit a velocity impulse is applied to the vehicle which results in impact on the earth. The analysis considers the problem of determining the magnitude and direction of the velocity impulse required to produce impact at a specified range from the point of application of the impulse. In addition, the dispersion in range and deflection about the desired impact point is evaluated in terms of the capabilities of the vehicle propulsion and attitude control system as well as the satellite tracking system.

As an interesting by-product of this study, a velocity diagram was developed which provides a convenient tool for determining the subsequent characteristics of a trajectory as a function of the velocity and path direction corresponding to a given initial position. This diagram enables one to determine whether the resulting path escapes the earth's field, continues on a satellite orbit, or impacts on the earth. In addition, it determines the range to impact (if any) as well as the shape and orientation of the satellite orbits.

As a result of this study, the magnitude and direction of the change in velocity needed to produce impact have been so optimized as to require a minimum impulse and at the same time to give a minimum value of the dispersion.

CONTENTS

SYMBOLS

C	Nondimensional measure of orbital angular momentum
ΔD	Deflection error in impact
g_o	Gravitational acceleration at the earth's surface
h_o	Altitude of the initial point
R	Range to impact
R_o	Earth's radius
ΔR	Range error in impact
r	Radius vector measured from the earth's center
r_o	Value of r at the initial point
t	Time
V	Vehicle velocity
V_l	Vehicle velocity change
V_{ln}	Component of V_l normal to the desired direction and in the trajectory plane
V_{lz}	Component of V_l normal to the trajectory plane
V_n	Component of V_o normal to the desired direction and in the trajectory plane
V_o	Resultant vehicle velocity after impulse
V_s	Satellite orbital velocity prior to impulse
V_{sn}	Component of V_s normal to the desired direction and in the orbital plane
V_{sz}	Component of V_s normal to the orbital plane
V_z	Component of vehicle velocity normal to the trajectory plane
ΔV_l	Error in V_l
ΔV_{ln}	Error in V_{ln}
ΔV_{lz}	Error in V_{lz}

ΔV_n Error in V_n

ΔV_o Error in V_o

ΔV_s Error in V_s

ΔV_{sn} Error in V_{sn}

ΔV_{sz} Error in V_{sz}

ΔV_z Error in V_z

v Nondimensional measure of V

v_1 Nondimensional measure of V_1

v_c Nondimensional measure of circular orbital velocity

v_e Nondimensional measure of escape velocity

v_m Nondimensional measure of the velocity to produce a perigee or apogee radius x_m

v_o Nondimensional measure of V_o

v_p Nondimensional measure of the velocity for zero perigee altitude

v_x Horizontal component of v_o

v_y Vertical component of v_o

x Nondimensional measure of r

x_m Value of x at apogee or perigee

x_o Value of x at the initial point

Δz Position error normal to the trajectory plane

α Direction of velocity change relative to the horizontal

$\Delta\alpha$ Error in α

γ Trajectory path angle

γ_1 Value of γ at impact

γ_m Value of γ at the initial point to give an apogee or perigee radius x_m

γ_o	Path angle of trajectory at the initial point after impulse
γ_p	Path angle for zero perigee path
γ_s	Path angle of satellite just prior to impulse
$\Delta\gamma_s$	Error in γ_s
θ	Range angle measured from x_o
θ_1	Range angle to impact
θ_m	Range angle to apogee
θ_o	Range angle of the initial point
$\Delta\theta_o$	Error in θ_o

I. INTRODUCTION

It is the purpose of this report to investigate the capabilities of a recoverable satellite with regard both to the change in velocity required to cause impact on the earth and to the accuracy with which the impact point can be predicted. While this problem was considered in Ref. 1 for the specific case of recovery from a circular satellite orbit, the present report gives a more general treatment of the problem.

The approach used in this analysis was to assume a satellite vehicle which has on board a propulsion system capable of producing an impulsive velocity change of any desired magnitude and direction. If this vehicle is in orbit, either elliptical or circular, the recovery process can be initiated by the application of an appropriate velocity impulse at any point of the orbit. This initiation point is characterized by a radial distance from the center of the earth, r_o, a vehicle velocity, V_s, and a path direction relative to the horizontal, γ_s. Since no limitation has been placed on the magnitude or direction of the applied impulse, it is then possible to achieve any resultant velocity, V_o, and path direction, γ_o, after the application of the impulse with the same value of radial distance r_o. Thus the behavior of the vehicle subsequent to the velocity change is described by determining the trajectory corresponding to the initial conditions r_o, V_o, and γ_o.

Section II presents the desired trajectory characteristics by means of a velocity diagram which shows, for a given r_o, the ranges of V_o and γ_o corresponding to impact trajectories, satellite orbits, and escape paths. Included in this diagram are contours of constant angular range from initial point to impact as well as contours of constant apogee and perigee height for satellite orbits.

Section III determines the minimum velocity change required to impact at a given angular range from the initial point, and also specifies the values of the dispersion derivatives for range and deflection resulting from uncertainties in the magnitude and direction of the velocity change.

Sections IV and V summarize the results and conclusions of this analysis and indicate further work which is necessary to refine the results of this study.

II. TRAJECTORY CHARACTERISTICS

As indicated in the introduction, this section considers the type of path which a vehicle follows when its initial conditions are specified by an initial radial distance, r_o, an initial velocity, V_o, and an initial path angle, γ_o.

SPECIFICATION OF PROBLEM

The geometry of the problem is shown in Fig. 1, where the symbols are self-explanatory. However, to handle the problem analytically, it is convenient to make use of nondimensional variables defined as follows:

$$v = \frac{V}{\sqrt{R_o g_o}} \tag{1}$$

$$x = \frac{r}{R_o} \tag{2}$$

where R_o is the radius of the earth and g_o is the gravitational constant at the earth's surface.

BASIC TRAJECTORY EQUATIONS

In terms of the given initial conditions the basic trajectory equations are given in Ref. 2 as follows:

$$\frac{1}{x} = \frac{1}{C^2} + \left(\frac{1}{x_o} - \frac{1}{C^2}\right) \cos\theta - \frac{\tan \gamma_o}{x_o} \sin\theta \tag{3}$$

$$\tan \gamma = x \left[\left(\frac{1}{x_o} - \frac{1}{C^2}\right) \sin\theta + \frac{\tan \gamma_o}{x_o} \cos\theta \right] \tag{4}$$

where

$$C = x_o v_o \cos \gamma_o \tag{5}$$

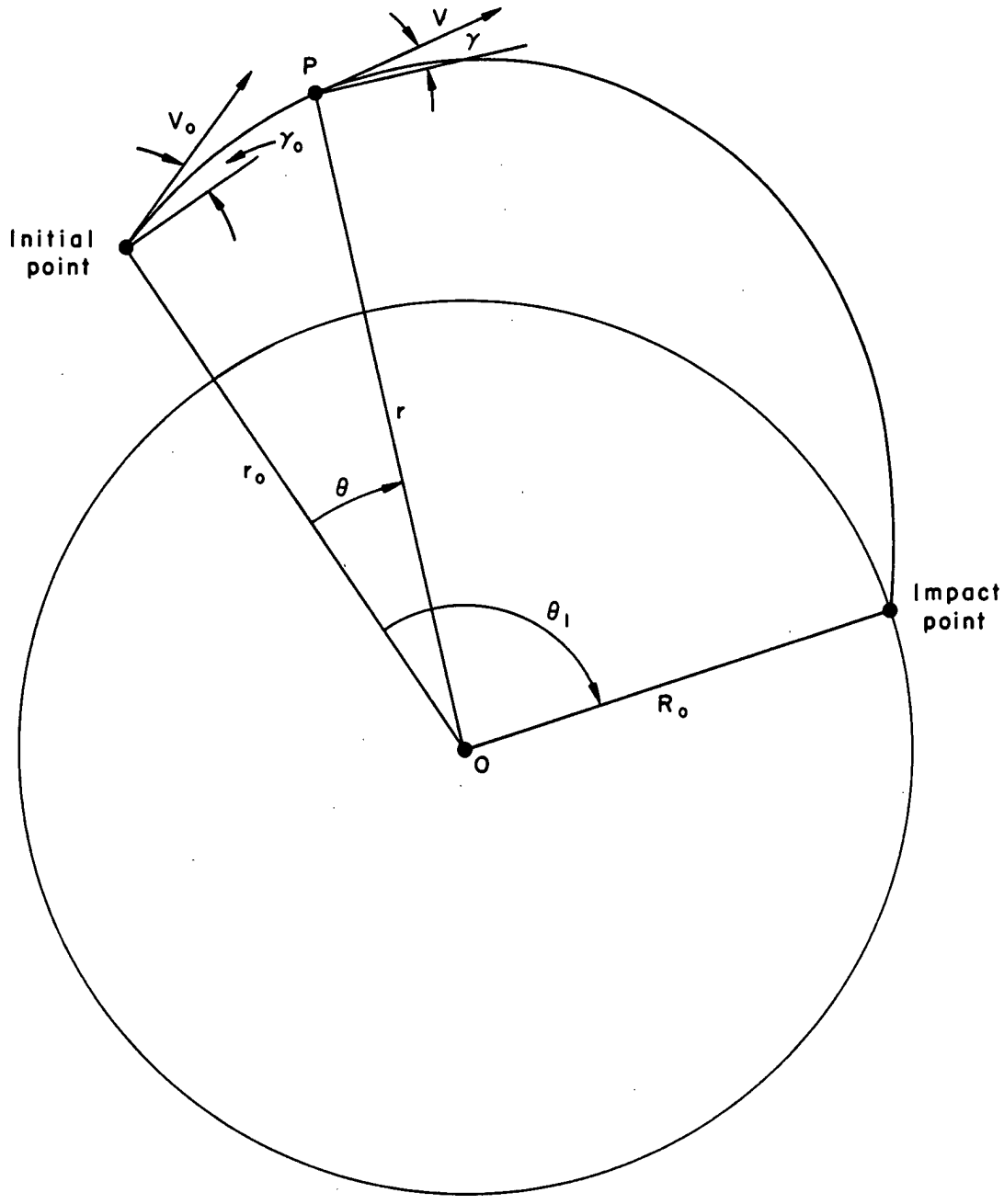

Fig. 1 — Geometry of the problem

and vacuum trajectories relative to a spherical nonrotating earth are assumed.

VELOCITY DIAGRAM

A convenient method of presenting the trajectory characteristics is by means of a velocity diagram in which the rectangular coordinates are the x and y components (horizontal and vertical) of the initial velocity vector (v_o, γ_o). Thus the radial distance from the origin to any point in the v_x, v_y plane represents a possible initial velocity vector. If the value of the initial radial distance as specified by x_o is held fixed, then the v_x, v_y plane can be divided into regions by the limiting contours described below.

Limiting Contours

Escape Condition. One significant contour in the velocity diagram is the boundary between escape and non-escape conditions. In terms of the non-dimensional variables the value of escape velocity is given by

$$v_e^2 = \frac{2}{x_o} \tag{6}$$

Thus the boundary curve in the velocity diagram is given by the relation

$$v_x^2 + v_y^2 = \frac{2}{x_o} \tag{7}$$

which is a circle about the origin with a radius equal to $\sqrt{2/x_o}$. Any velocity vector that terminates on or outside this circle corresponds to either a parabolic or a hyperbolic escape path, while any vector that terminates inside this circle corresponds to either an impact or a satellite path.

Zero Perigee Altitude Condition. A second limiting contour can be determined as follows. Suppose that an impact point is selected beyond the

horizon at a range angle θ_1. Obviously there are an infinite number of combinations of v_o and γ_o which will result in impact at the desired position. However, as the value of γ_o is decreased and v_o is varied to maintain the range θ_1, the value of the path angle at impact, γ_1, becomes smaller until finally a combination of γ_o and v_o is reached for which γ_1 is zero. This path can be described as either an impact trajectory with grazing incidence at the target or a satellite orbit with a zero perigee altitude at a range angle θ_1. At any rate the vector (v_o, γ_o) which produces this path specifies a point on the contour dividing satellite vehicles from impacting vehicles in the velocity diagram. If this vector is defined as $v_p(\theta_1)$, $\gamma_p(\theta_1)$, these values can be determined by substituting the following conditions in Eqs. (3), (4), and (5):

$$\left.\begin{aligned} v_o &= v_p \\ \gamma_o &= \gamma_p \end{aligned}\right\} \text{ at } \theta = 0$$

$$\left.\begin{aligned} x &= 1 \\ \gamma &= 0 \end{aligned}\right\} \text{ at } \theta = \theta_1$$

Solution of the resulting equations for v_p and γ_p gives

$$v_p^2 = \frac{2 - x_o}{x_o} + \frac{x_o - 1}{1 - x_o \cos \theta_1} \tag{8}$$

$$\tan \gamma_p = \frac{1 - x_o}{\tan \frac{\theta_1}{2}} \tag{9}$$

These parametric equations can be expressed in Cartesian coordinates by the following transformation

$$v_p^2 = v_x^2 + v_y^2 \tag{10}$$

$$\tan \gamma_o = \frac{v_y}{v_x} \tag{11}$$

Combination of Eqs. (8), (9), (10), and (11) gives the following expression for the contour of zero perigee altitude, where θ_1 varies along the curve:

$$\frac{x_o (1 + x_o)}{2} v_x^2 - \frac{x_o}{2 (x_o - 1)} v_y^2 = 1 \tag{12}$$

This contour is a hyperbola with its major axis along the v_x axis of the diagram and with asymptotes in the direction of the horizon as seen from the initial position.

Velocity Diagram Regions. If the two contours defined by Eqs. (7) and (12) are drawn on the velocity diagram, the configuration shown in Fig. 2 results. It should be noted that parts of these contours are dashed, since they have no significance for the purposes of this study. For instance, in the upper half-plane the parts of the hyperbola which extend beyond the circle represent escape paths which have a zero perigee altitude. However, this is a virtual perigee, since it occurs on the backward extension of the path from the initial point. Thus for all practical purposes these conditions are merely escape trajectories, since they are outside the circular contour.

On the other hand, in the lower half-plane the portions of the hyperbola beyond the circle represent escape paths with zero perigee altitude where perigee occurs prior to escape. Thus this contour still represents the boundary between escape and impact conditions. In addition the part of

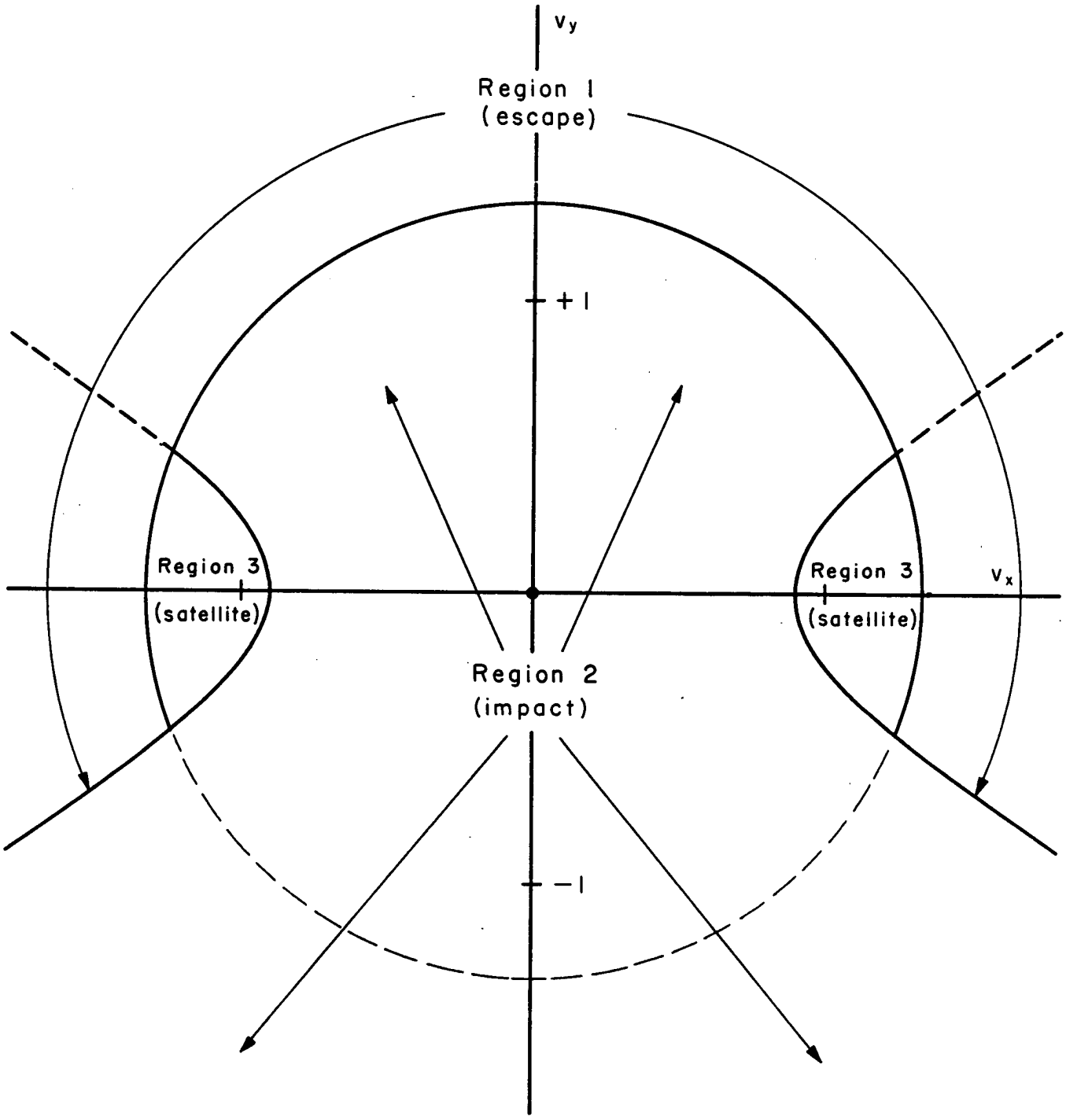

Fig. 2 — Velocity diagram regions

the circular contour between the two branches of the hyperbola has no significance, since the points below this contour represent escape paths which would have to pass through the earth before escape. Thus the region below the circular and hyperbolic contours can be considered as corresponding to impact trajectories.

Consequently, in Fig. 2 three regions can be specified with the following characteristics:

Region 1: The area outside the circular escape contour and above two lower branches of the hyperbola corresponds to escape trajectories.

Region 2: The area between the two branches of the hyperbola and below the upper half of the circular escape contour corresponds to trajectories which impact on the earth. This region is of infinite extent in the lower half-plane.

Region 3: This area is composed of the two parts of the plane between the circular contour and each branch of the hyperbola and corresponds to satellite orbital conditions.

In the velocity diagram described, points in the left half-plane correspond to paths with move in a counterclockwise direction, while points in the right half-plane represent paths in a clockwise direction. In view of the symmetry, only the right half-plane will be shown in future diagrams in this report.

Variation of Initial Altitude. As indicated previously, the velocity diagram described above is drawn for a particular value of the initial radial distance, x_o. Unfortunately this diagram does not scale conveniently with a variation in x_o, and Fig. 3 shows how the limiting contours vary as

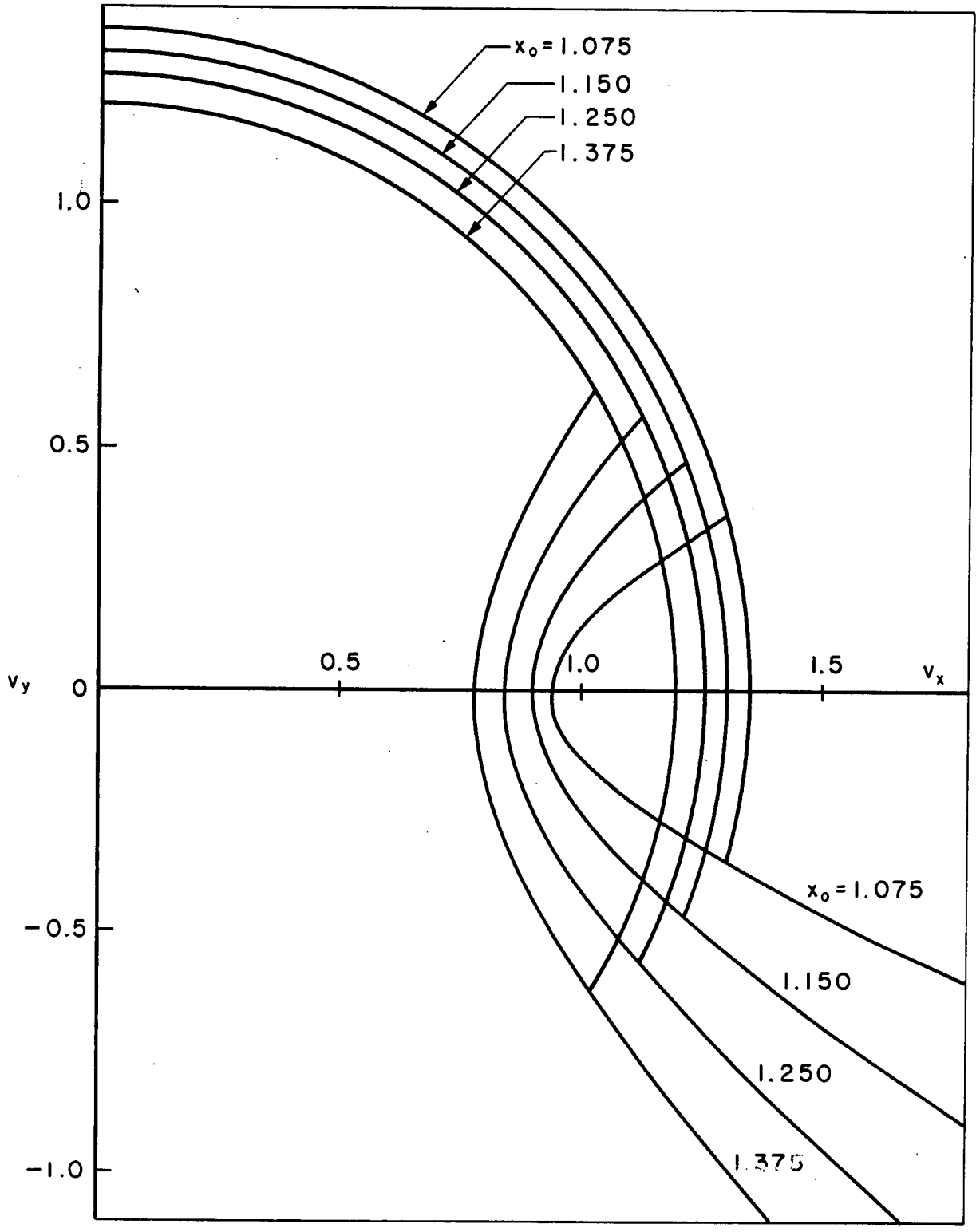

Fig. 3 — Velocity diagram as a function of initial altitude

x_o is changed. Four cases are shown as specified in the following text table.

Case	h_o (stat mi)	r_o (stat mi)	x_o
1	300	4300	1.075
2	600	4600	1.150
3	1000	5000	1.250
4	1500	5500	1.375

An examination of Fig. 3 shows that the radius of the circular escape velocity contour decreases with altitude. At the same time, the hyperbolic contour widens and moves closer to the origin, with the result that the satellite region between these two curves increases in size.

Impact Trajectories

In Region 2, defining impact trajectories, it is desirable to indicate the position of impact corresponding to a given combination of v_o and γ_o. This can be done conveniently by drawing contours of constant angular range, θ_1, from initial point to impact. These contours can be determined as follows:

Range Contours. If the condition that $x = 1$ at $\theta = \theta_1$ is substituted in Eqs. (3) and (5), the following relationship results between v_o, γ_o, and θ_1:

$$v_o^2 = \frac{1 - \cos\theta_1}{x_o \cos\gamma_o \left[x_o \cos\gamma_o - \cos(\theta_1 + \gamma_o)\right]} \tag{13}$$

This can be put into Cartesian coordinates by the transformation

$$v_o^2 = v_x^2 + v_y^2 \tag{14}$$

$$\tan\gamma_o = \frac{v_y}{v_x} \tag{15}$$

Combination of Eqs. (13), (14), and (15) gives

$$v_y = \left(\frac{1 - \cos\theta_1}{x_o \sin\theta_1}\right) \frac{1}{v_x} - \left(\frac{x_o - \cos\theta_1}{\sin\theta_1}\right) v_x \qquad (16)$$

which is the expression for a contour of constant range, θ_1.

Limits on Range Contours. Inasmuch as the range contours resulting from Eq. (16) are only valid within Region 2, it is useful to specify the spread of values of v_x for which they should be evaluated. Figure 4 shows schematically the three types of contour which may result, depending upon the value of θ_1 selected.

Contour A results for impact points which are within line of sight of the initial point:

$$0 < \theta_1 < \cos^{-1}\left(\frac{1}{x_o}\right) \qquad (17)$$

These contours start on the circular escape contour and approach an asymptote in the lower half-plane in the direction of the line of sight from initial point to impact point. The spread of v_x to be considered is given by

$$\frac{\sin\frac{\theta_1}{2}}{x_o^{1/2}} \left[\frac{2}{1 + x_o + 2x_o^{1/2}\cos\frac{\theta_1}{2}}\right]^{1/2} < v_x < \infty \qquad (18)$$

Contour B results for impact positions beyond the horizon from the initial point but at range angles less than 180 deg:

$$\cos^{-1}\left(\frac{1}{x_o}\right) < \theta_1 < \pi \qquad (19)$$

These contours start on the escape boundary and terminate tangentially on the zero perigee contour. The spread of values of v_x is given by

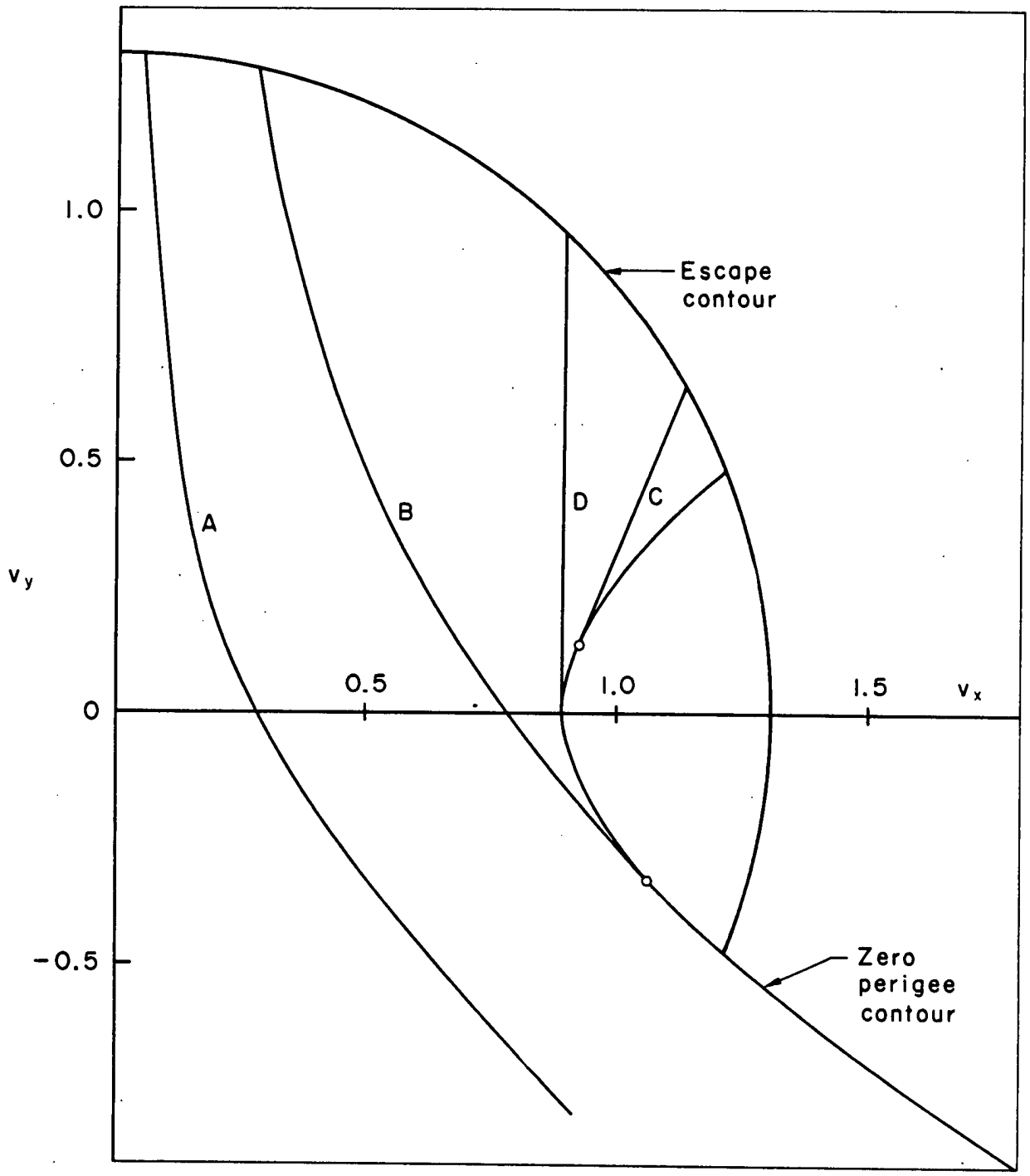

Fig. 4 — Range contour characteristics

$$\frac{\sin\frac{\theta_1}{2}}{x_o^{1/2}}\left[\frac{2}{1+x_o+2x_o^{1/2}\cos\frac{\theta_1}{2}}\right]^{1/2} < v_x < \left[\frac{1-\cos\theta_1}{x_o(1-x_o\cos\theta_1)}\right]^{1/2} \quad (20)$$

Contour C results for ranges from 180 deg to the maximum range attainable from the given initial point:

$$\pi < \theta_1 < 2\pi - \cos^{-1}\left(\frac{1}{x_o}\right) \quad (21)$$

These contours start tangentially from the zero perigee boundary and terminate at the escape contour. The corresponding spread for v_x is given by

$$\left[\frac{1-\cos\theta_1}{x_o(1-x_o\cos\theta_1)}\right]^{1/2} < v_x < \frac{\sin\frac{\theta_1}{2}}{x_o^{1/2}}\left[\frac{2}{1+x_o-2x_o^{1/2}\cos\frac{\theta_1}{2}}\right]^{1/2} \quad (22)$$

For values of θ_1 such that

$$\theta_1 > 2\pi - \cos^{-1}\left(\frac{1}{x_o}\right)$$

no trajectory in a clockwise sense exists which can result in impact from the selected initial point.

Contour D is the contour for $\theta_1 = \pi$ and is always a vertical line tangent to the vertex of the hyperbola and independent of the value of x_o.

Figure 5 gives a detailed plot of the range contours for Case 2 of the text table above, for 10-deg increments in the range angle.

Satellite Orbits

In Region 3, corresponding to satellite orbits, the principal orbit characteristics of interest for this study are the perigee altitude, the

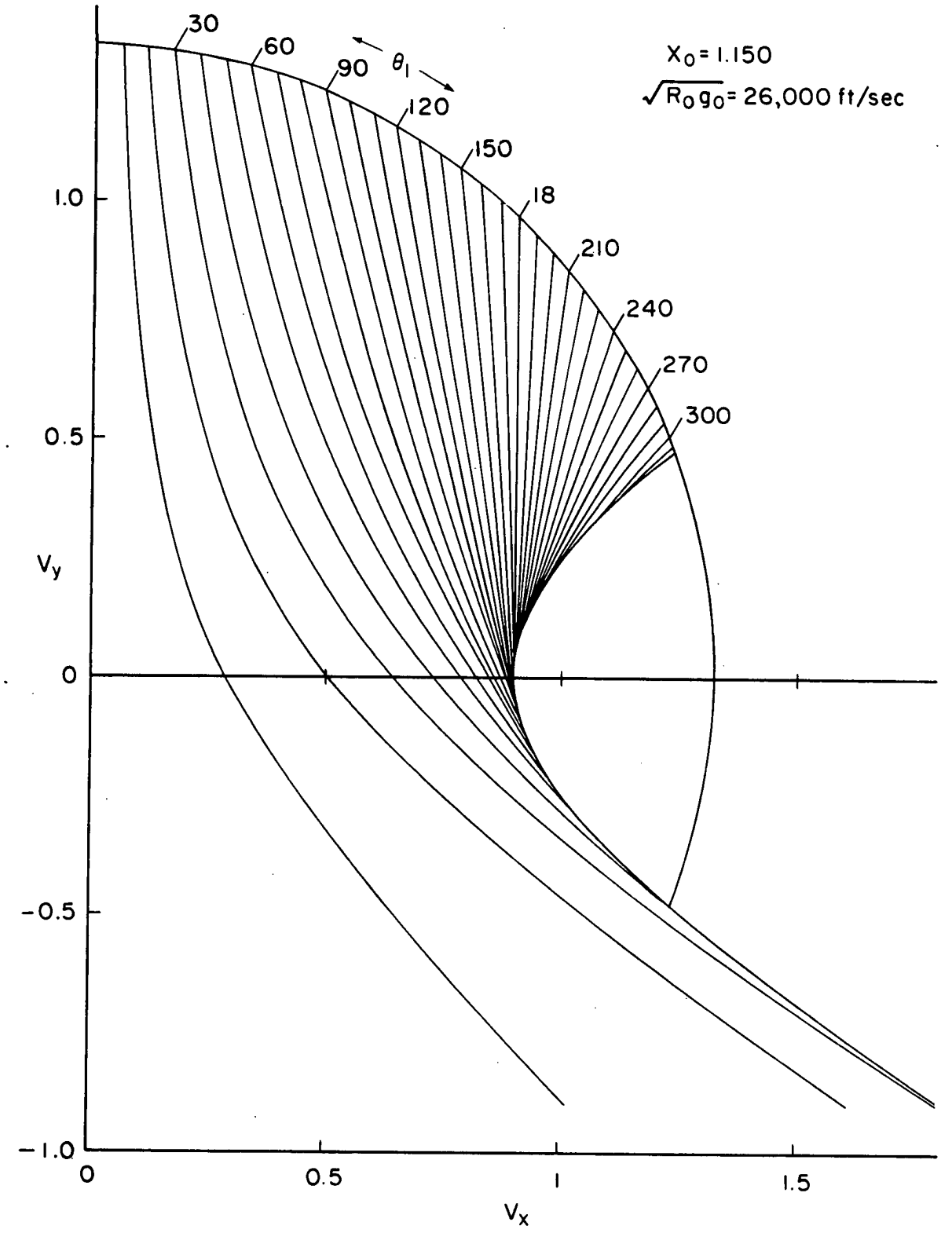

Fig. 5 — Range contours

the apogee altitude, and the orientation of the orbit in the plane relative to the initial position. These quantities are determined as follows:

Contours of Constant Perigee Height. If the vector (v_m, γ_m) represents the velocity at x_o which will produce a radial distance, x_m, to perigee at a range angle θ_m from the initial point, a contour of constant x_m can be determined as follows:

Let

$$\left.\begin{aligned} v_o &= v_m \\ \gamma_o &= \gamma_m \end{aligned}\right\} \text{ at } \theta = 0$$

$$\left.\begin{aligned} x &= x_m \\ \gamma &= 0 \end{aligned}\right\} \text{ at } \theta = \theta_m$$

Substitution of the above conditions in Eqs. (3), (4), and (5) gives the following relation for v_m and γ_m as functions of θ_m and x_o/x_m:

$$v_m^2 = \frac{2 - \frac{x_o}{x_m}}{x_o} + \frac{\frac{x_o}{x_m}\left(\frac{x_o}{x_m} - 1\right)}{x_o\left[1 - \frac{x_o}{x_m}\cos\theta_m\right]} \tag{23}$$

$$\tan\gamma_m = \frac{1 - \frac{x_o}{x_m}}{\tan\frac{\theta_m}{2}} \tag{24}$$

By means of the transformation

$$v_m^2 = v_x^2 + v_y^2 \tag{25}$$

$$\tan\gamma_m = \frac{v_y}{v_x} \tag{26}$$

Eqs. (23) and (24) can be expressed in Cartesian coordinates in the form

$$\frac{x_o\left(1+\frac{x_o}{x_m}\right)}{2}\,v_x^2 - \frac{x_o}{2\left(\frac{x_o}{x_m}-1\right)}\,v_y^2 = 1 \qquad (27)$$

For values of $x_m < x_o$, this equation represents a contour of constant radial distance to perigee, x_m, and has the form of a hyperbola. For zero perigee altitude ($x_m = 1$), Eq. (27) reduces to Eq. (12), the limiting contour between impact trajectories and satellite orbits. As the value of x_m increases toward x_o, these hyperbolas become narrower and their vertices move to the right. In the limit when $x_m = x_o$, the hyperbola reduces to a segment of the v_x axis from the position of circular orbital velocity.

$$v_x = \sqrt{\frac{1}{x_o}} \qquad (28)$$

to the escape velocity

$$v_x = \sqrt{\frac{2}{x_o}} \qquad (29)$$

Figure 6 is an enlarged plot of the satellite region and shows the constant perigee contours for perigee altitudes of 0, 100, 200, 300, 400, 500, and 600 stat mi for Case 2 of the text table.

Contours of Constant Apogee Height. The contours of constant apogee are determined from Eq. (27) for values of $x_m > x_o$. Under these conditions the contours are ellipses, and for infinite apogee Eq. (27) reduces to Eq. (7), the circular contour between escape and satellite paths. As x_m becomes smaller, these ellipses become narrower and their vertices move to the left. In the limit as $x_m = x_o$ the ellipse reduces to a segment on the v_x axis extending from the circular orbital position

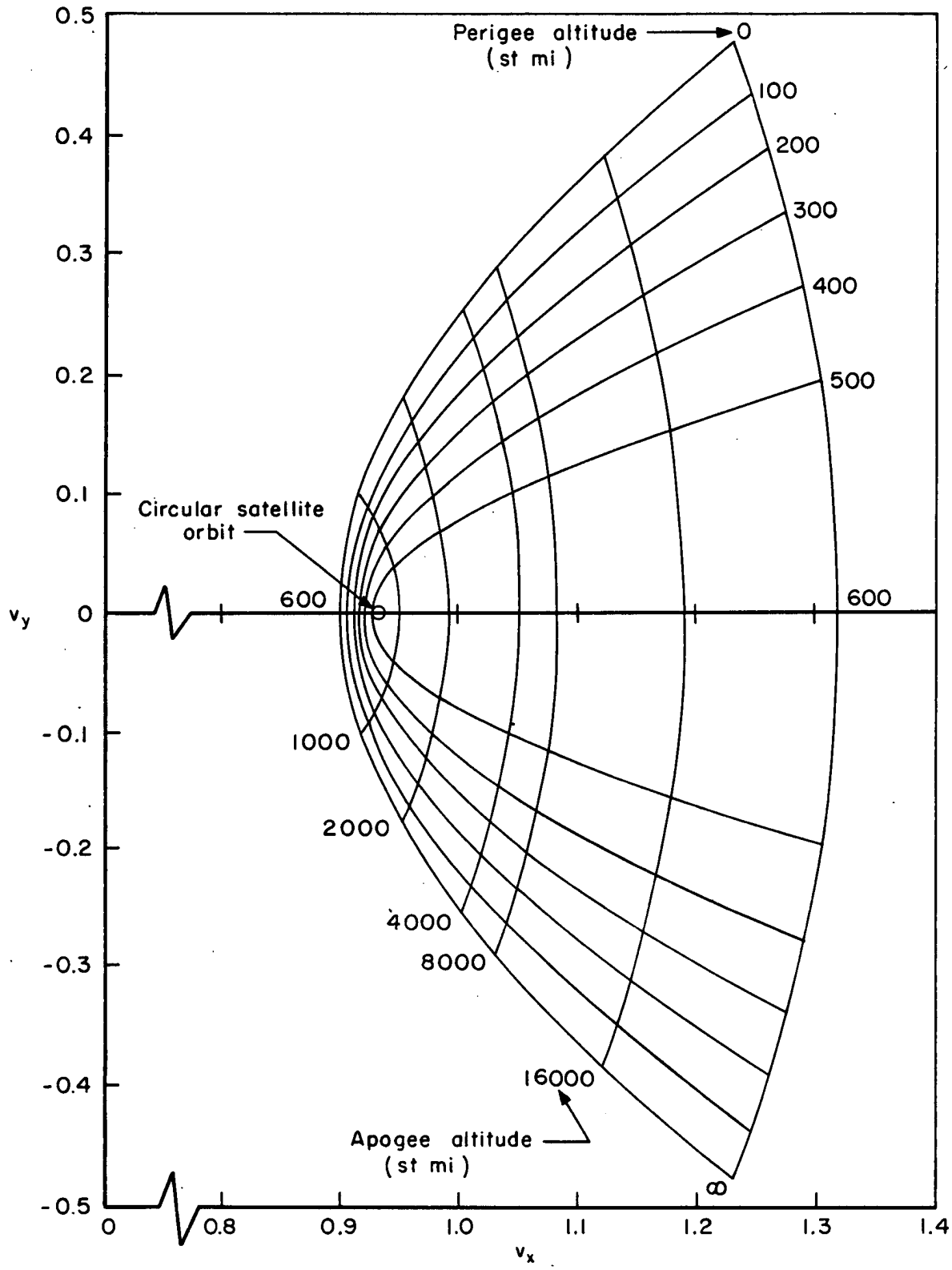

Fig. 6 — Contours of constant perigee and apogee altitudes (case 2)

$$v_x = \sqrt{\frac{1}{x_o}} \tag{30}$$

to the vertex of the zero perigee contour at

$$v_x = \sqrt{\frac{2}{x_o (x_o + 1)}} \tag{31}$$

These contours are also shown in Fig. 6 for apogee altitudes of 600, 1000, 2000, 4000, 8000, and 16,000 stat mi, again for Case 2 of the text table.

Contours of Constant Angular Position of Apogee These contours are obtained by eliminating $\frac{x_o}{x_m}$, γ_m, and v_m between Eqs. (23), (24), (25), and (26) to give

$$v_y = \frac{\tan\theta_m}{x_o^{1/2}} \left[\frac{1}{x_o^{1/2} v_x} - x_o^{1/2} v_x \right] \tag{32}$$

The contours have the same functional form with regard to v_x, while the angular position, θ_m, enters as a multiplying factor, tan θ_m. Figure 7 is an enlarged plot of the satellite region showing these contours for 10-deg steps in θ_m from zero to 360 deg, evaluated for Case 2 of the text table.

Remarks

Actually in the velocity diagram as developed in this section and as shown in Figs. 5 through 7, the contours of constant apogee height and angular position could be extended into Region 2 for impact trajectories. However, it was not felt that these data were particularly significant for this region.

The diagram as presented provides a convenient method for determining the behavior of a vehicle with given initial conditions of x_o, v_o, and γ_o.

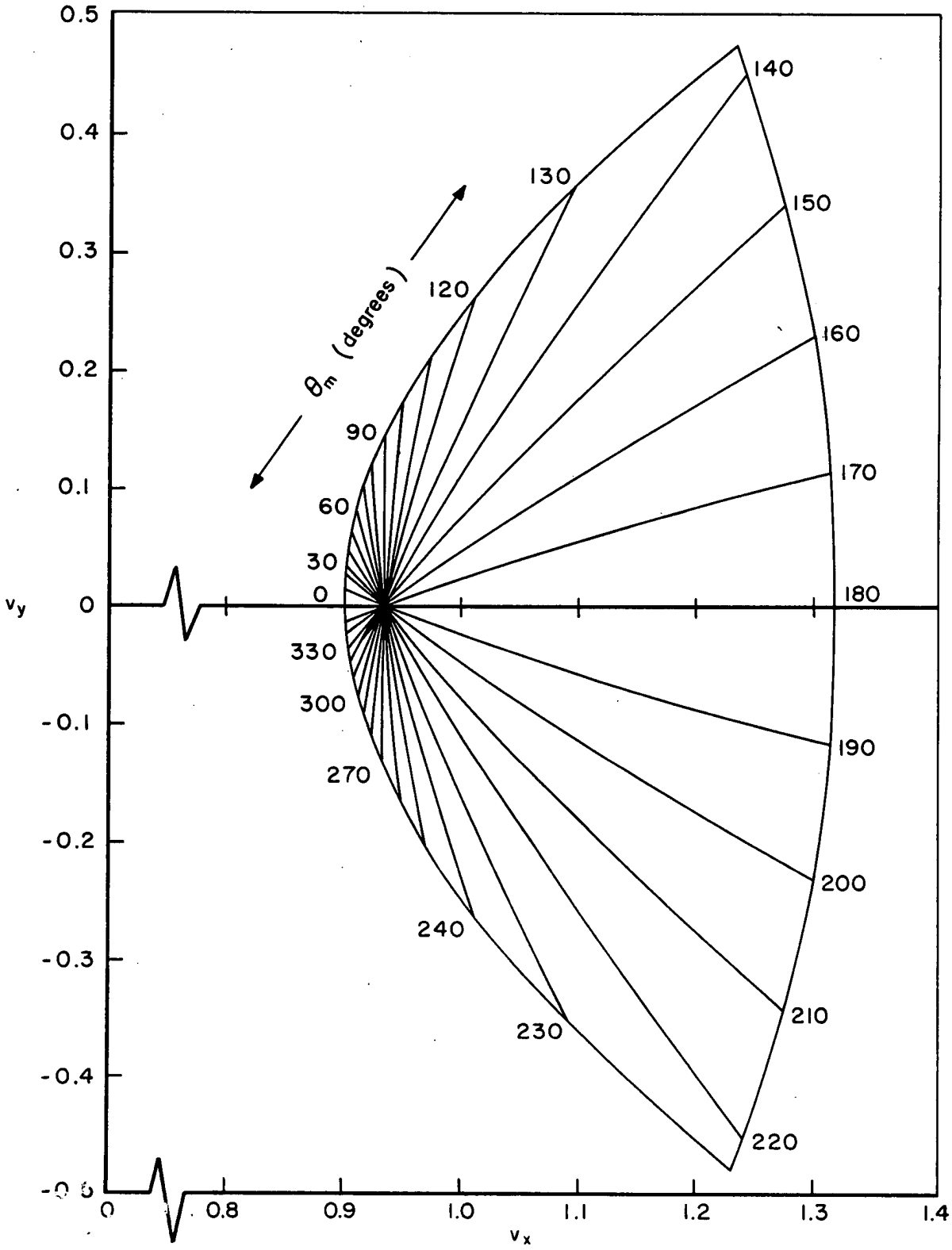

Fig. 7 —— Contours of constant angular position of apogee (case 2)

It is also a simple matter to determine the magnitude of the velocity change required to change from a satellite orbit through the initial point to an impact-type trajectory.

III. SATELLITE RECOVERY CAPABILITIES

In the previous section, the velocity diagram was developed to specify the type of path which a vehicle would follow with a resultant velocity (v_o, γ_o) from an initial radial distance, x_o. The present section uses this diagram to determine the velocity change required at x_o to change from a satellite orbit to an impact trajectory, and determines the accuracy with which the impact point can be predicted.

INITIAL ORBITAL CONDITIONS

For the present analysis, it is assumed that initially the vehicle is on a circular orbit at altitude x_o with a velocity

$$v_c = \sqrt{\frac{1}{x_o}} \tag{33}$$

While a circular orbit is assumed for convenience, the method of analysis is equally applicable to any elliptical orbit through the initial point, x_o. Also, it should be noted from Fig. 6 that an orbit must have a considerable eccentricity before the representative point in the velocity diagram deviates very much from the circular orbit condition. On the assumption of an initial circular or near-circular orbit, the geometry of the velocity change is shown in Fig. 8, where v_c is the circular orbital velocity, (v_1, α) is the velocity impulse, and (v_o, γ_o) is the resultant velocity after impulse, which is used in the velocity diagram to determine the subsequent behaviour of the vehicle.

MINIMUM IMPULSE REQUIREMENTS

Although in the introduction it was assumed that the propulsion system on board the vehicle had unlimited capability to produce changes in velocity,

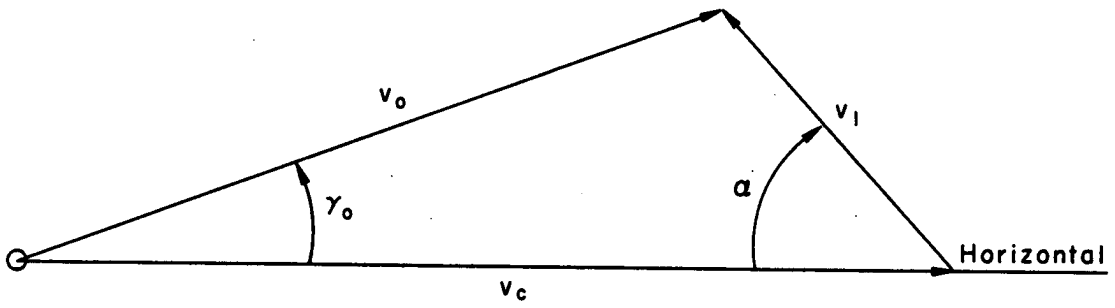

Fig. 8 — Geometry of velocity change

it is obviously desirable to minimize the magnitude of the velocity change in order to economize on the weight and space requirements for this propulsion system. An examination of the range contours in Fig. 5 shows that for values of range angle, θ_1, less than 180 deg a minimum value of v_1 as a function of θ_1 does exist with a direction of application downward and to the rear ($-\frac{\pi}{2} < \alpha < 0$). For values of the range angle, θ_1, greater than 180 deg the minimum v_1 is simply the vector which connects the circular orbital point with the terminus of the range contour at the zero perigee limit. In this case the minimum v_1 has an upward direction ($0 < \alpha < \pi$). However, from the point of view of accuracy the cases corresponding to ranges less than 180 deg are more favorable and will be analyzed in more detail in the following paragraphs.

To determine the minimum value of v_1 corresponding to a given value of range angle, θ_1, let the distance v_1 from the circular orbital point to a point (v_x, v_y) of the θ_1 range contour be given by

$$v_1^2 = (v_c - v_x)^2 + v_y^2 \tag{34}$$

and the condition for a minimum value of v_1 by

$$\frac{dv_1^2}{dv_x} = 0 \tag{35}$$

Then combination of Eqs. (16), (33), (34), and (35) gives the following relation for v_x, corresponding to minimum v_1:

$$v_x^4 - \frac{v_c \sin^2\theta_1}{1 + x_o^2 - 2x_o\cos\theta_1} v_x^3 - \frac{(1 - \cos\theta_1)^2}{x_o^2 (1 + x_o^2 - 2x_o\cos\theta_1)} + 0 \tag{36}$$

Numerical solution of Eqs. (16), (34), and (36) gives the desired minimum value of v_1, while the corresponding values of γ_o and α are given by

$$\tan \gamma_o = \frac{v_y}{v_x} \tag{37}$$

$$\tan \alpha = \frac{v_y}{v_c - v_x}$$

Figure 9 shows the loci of these minimum values of v_1 for each of the four cases in the text table, as well as the position of the circular orbital point for each case. It is seen that in general the velocity change required is downward and to the rear. As the value of x_o increases the required changes are increasingly to the rear.

In addition a cross plot of contours of constant range angle, θ_1, is shown for range angles between 10 and 90 deg.

RANGE DISPERSION

In order to determine the sensitivity of the impact position to errors in the initial conditions, the relations developed in Ref. 3 for the various dispersion derivatives are applied to the present case. It is assumed that accurate tracking data for the satellite orbit are available prior to the initiation of the recovery process; thus errors in impact position will be due primarily to errors in the resultant velocity and path direction after velocity change. The appropriate dispersion derivatives from Ref. 3 are given by

$$\frac{\partial R}{\partial V_o} = 2\sqrt{\frac{R_o}{g_o}} \; \frac{\sin \frac{\theta_1}{2}\left[x_o \cos \gamma_o - \cos (\theta_1 + \gamma_o)\right]}{v_o \left[x_o \cos\gamma_o \cos \frac{\theta_1}{2} - \cos \left(\frac{\theta_1}{2} + \gamma_o\right)\right]} \tag{39}$$

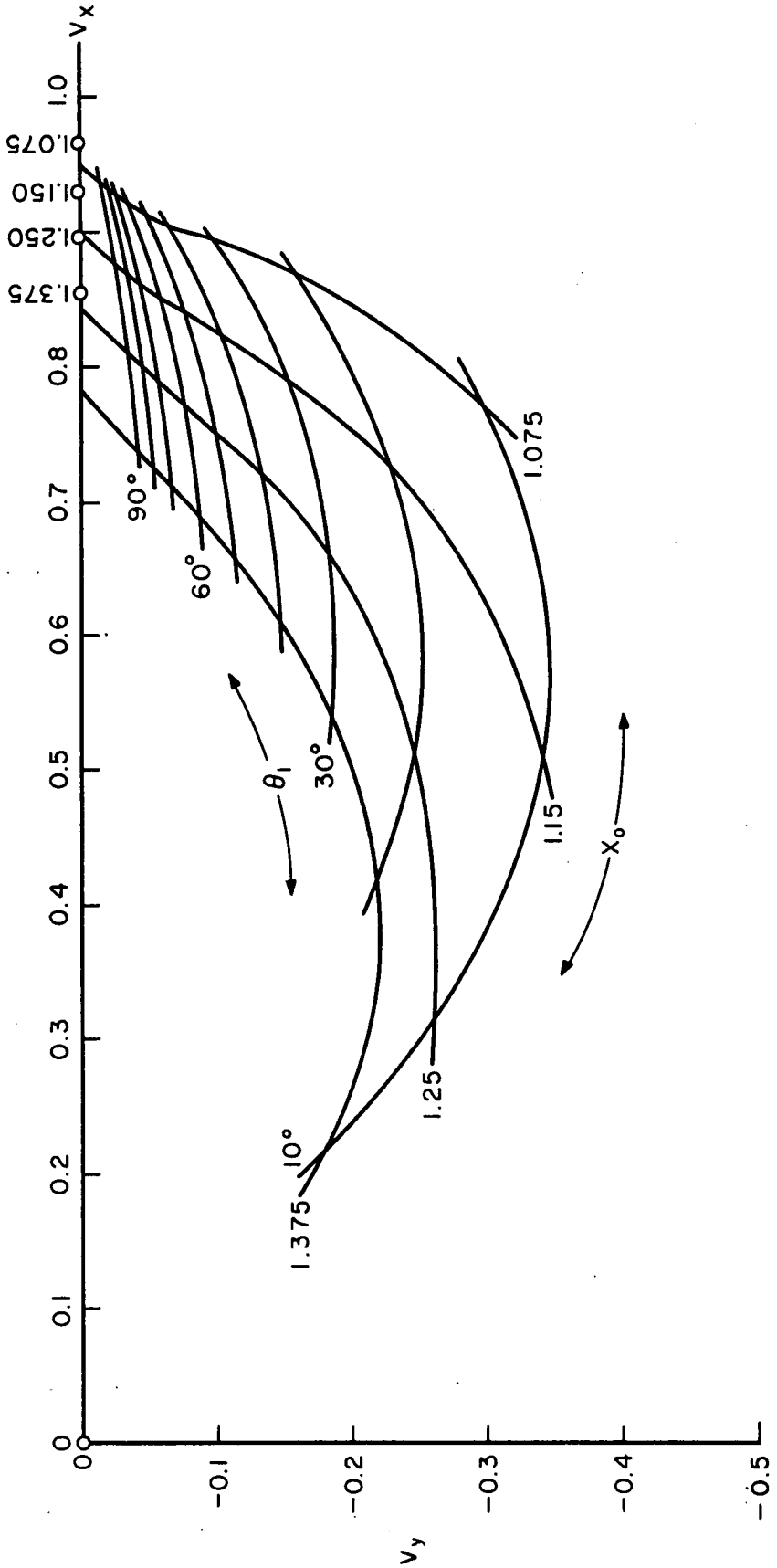

Fig.9—Conditions for minimum velocity change

$$\frac{\partial R}{\partial V_n} = \sqrt{\frac{R_o}{g_o}} \; \frac{\sin \frac{\theta_1}{2} \left[\sin (\theta_1 + 2\gamma_o) - 2x_o \sin\gamma_o \cos\gamma_o \right]}{v_o \cos\gamma_o \left[x_o \cos\gamma_o \cos \frac{\theta_1}{2} - \cos \left(\frac{\theta_1}{2} + \gamma_o \right) \right]} \tag{40}$$

where

$$v_o^2 = \frac{1 - \cos \theta_1}{x_o \cos\gamma_o \left[x_o \cos\gamma_o - \cos (\theta_1 + \gamma_o) \right]} \tag{41}$$

Equations (39) and (40) give the variation in range corresponding to errors in the magnitude and direction of the resultant velocity, V_o, in the trajectory plane. In view of the fact that it has already been assumed that good tracking data are available for the satellite orbit, then errors in the magnitude and direction of V_o are primarily due to uncertainties in the magnitude and direction of the velocity change, V_1. Thus the dispersion derivatives derivatives can be expressed as follows.

$$\frac{\partial R}{\partial V_1} = - \frac{\partial R}{\partial V_o} \cos (\alpha + \gamma_o) + \frac{\partial R}{\partial V_n} \sin (\alpha + \gamma_o) \tag{42}$$

$$\frac{\partial R}{\partial V_{1n}} = \frac{\partial R}{\partial V_o} \sin (\alpha + \gamma_o) + \frac{\partial R}{\partial V_n} \cos (\alpha + \gamma_o) \tag{43}$$

where V_{1n} is the component of V_1 normal to the desired direction of V_1 and in the trajectory plane.

If Eqs. (42) and (43) are evaluated for the cases of minimum V_1 determined above, it is seen that

$$\frac{\partial R}{\partial V_{1n}} = 0 \tag{44}$$

since the minimum velocity V_1 is normal to the particular range contour; thus to a first-order approximation the range is independent of small errors in the direction of V_1. Figures 10, 11, 12, and 13 present plots of the $\frac{\partial R}{\partial V_1}$ and the minimum v_1 as a function of range for range angles from zero to 90 deg for the four cases of the text table.

DEFLECTION DISPERSION

As to the effects of velocity uncertainties normal to the trajectory plane, Ref. 3 gives the following relation:

$$\frac{\partial D}{\partial V_z} = \sqrt{\frac{R_o}{g_o}} \quad \frac{\sin \theta_1}{v_o \cos \gamma_o} \tag{45}$$

where D is the deflection error of the impact position and V_z is the component of V_1 normal to the desired trajectory plane. Figure 14 shows a plot of Eq. (45) for the four cases of the text table. It should be noted that the values of $\frac{\partial D}{\partial V_z}$ rise sharply at short ranges. This is due to the increase in time to impact for these cases, and as a result it is probably undesirable to attempt to achieve impact ranges less than about 10 deg.

RANGE AND DEFLECTION ERRORS

On the basis of the assumption made above, the errors in range and deflection at the impact point are given by

$$\Delta R = \frac{\partial R}{\partial V_1} \quad \Delta V_1 \tag{46}$$

$$\Delta D = \frac{\partial D}{\partial V_z} \quad \Delta V_z \tag{47}$$

However, in order to evaluate these expressions, it is necessary to have a more detailed picture of the vehicle attitude and propulsion control system before significant results can be computed from Eqs. (46) and (47) to give a value of the circular probable error.

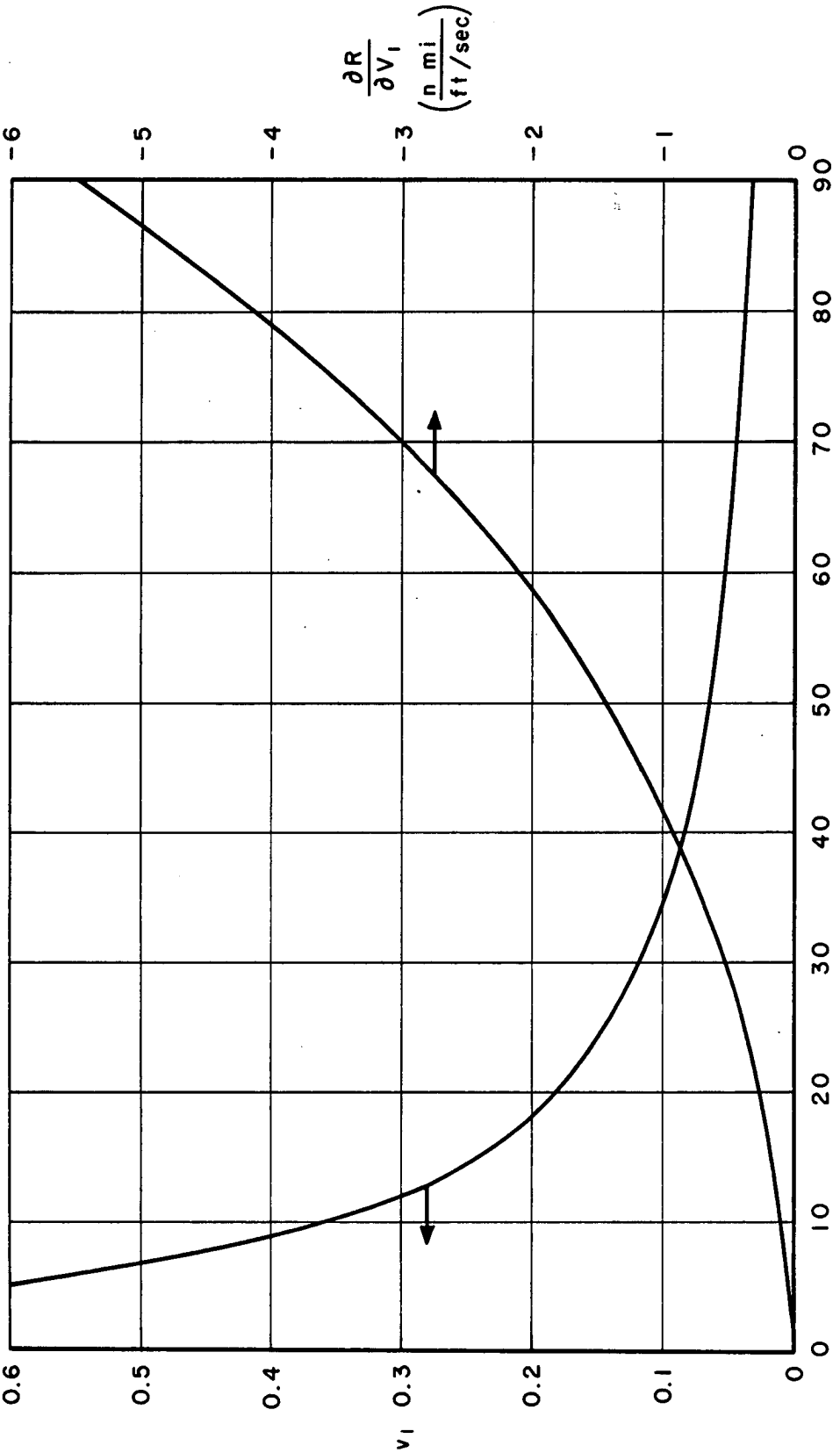

Fig. 10 — $\frac{\partial R}{\partial V_1}$ and minimum V_1 vs range angle (Case 1)

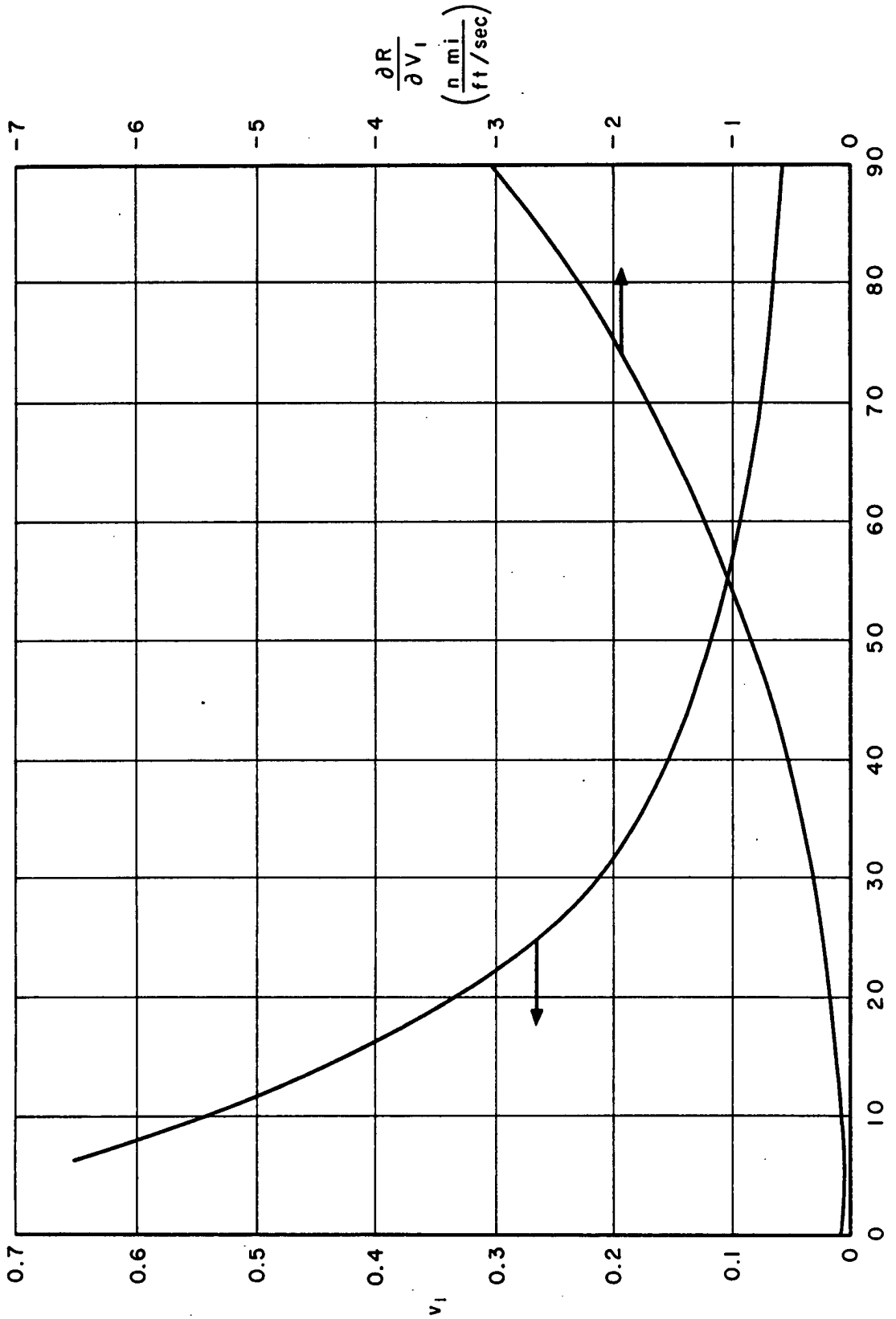

Fig. 11 — $\frac{\partial R}{\partial V_1}$ and minimum V_1 vs range angle (Case 2)

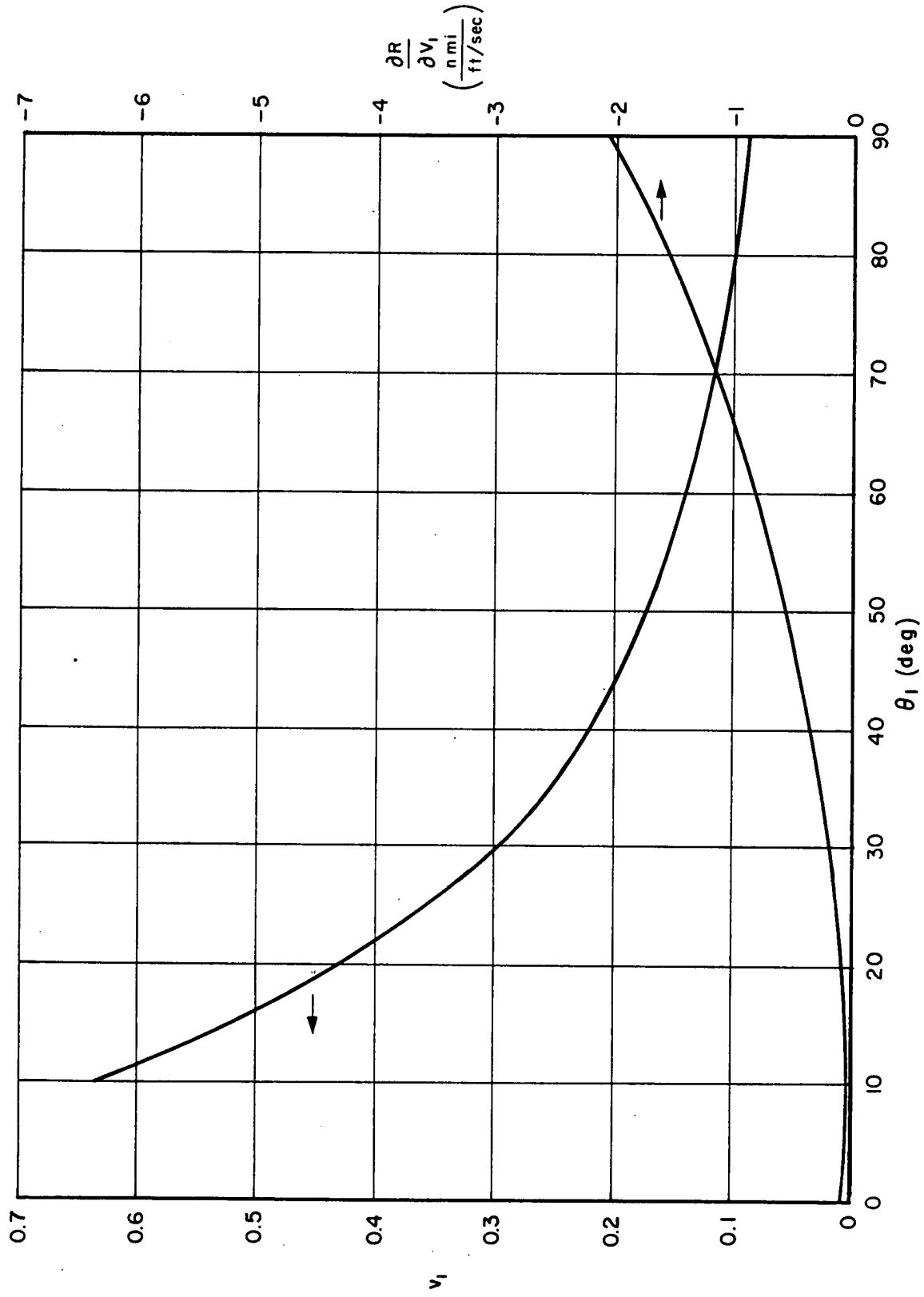

Fig.12 — $\frac{\partial R}{\partial V_1}$ and minimum V_1 vs range angle (Case 3)

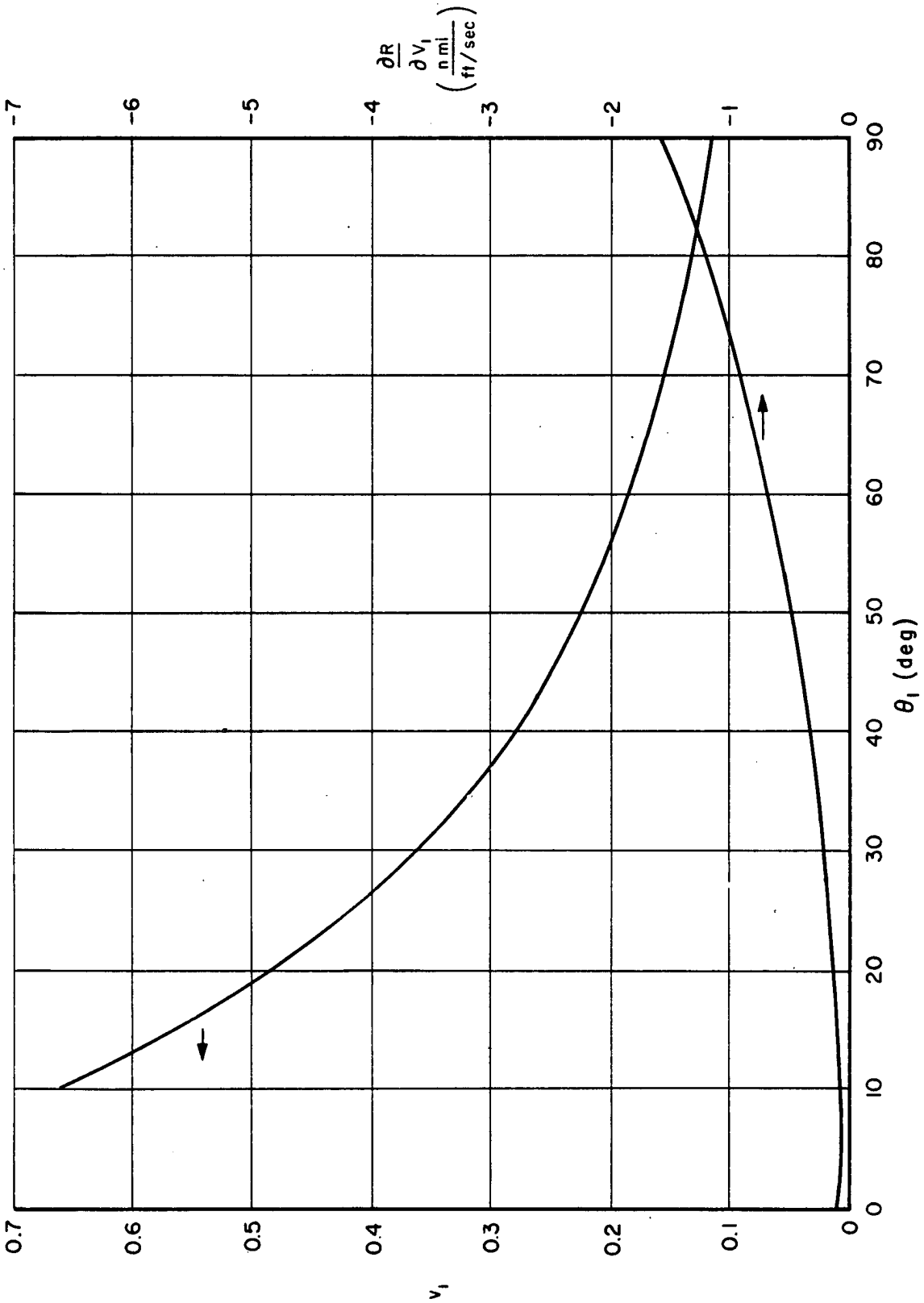

Fig.13 — $\frac{\partial R}{\partial V_1}$ and minimum V_1 vs range angle (Case 4)

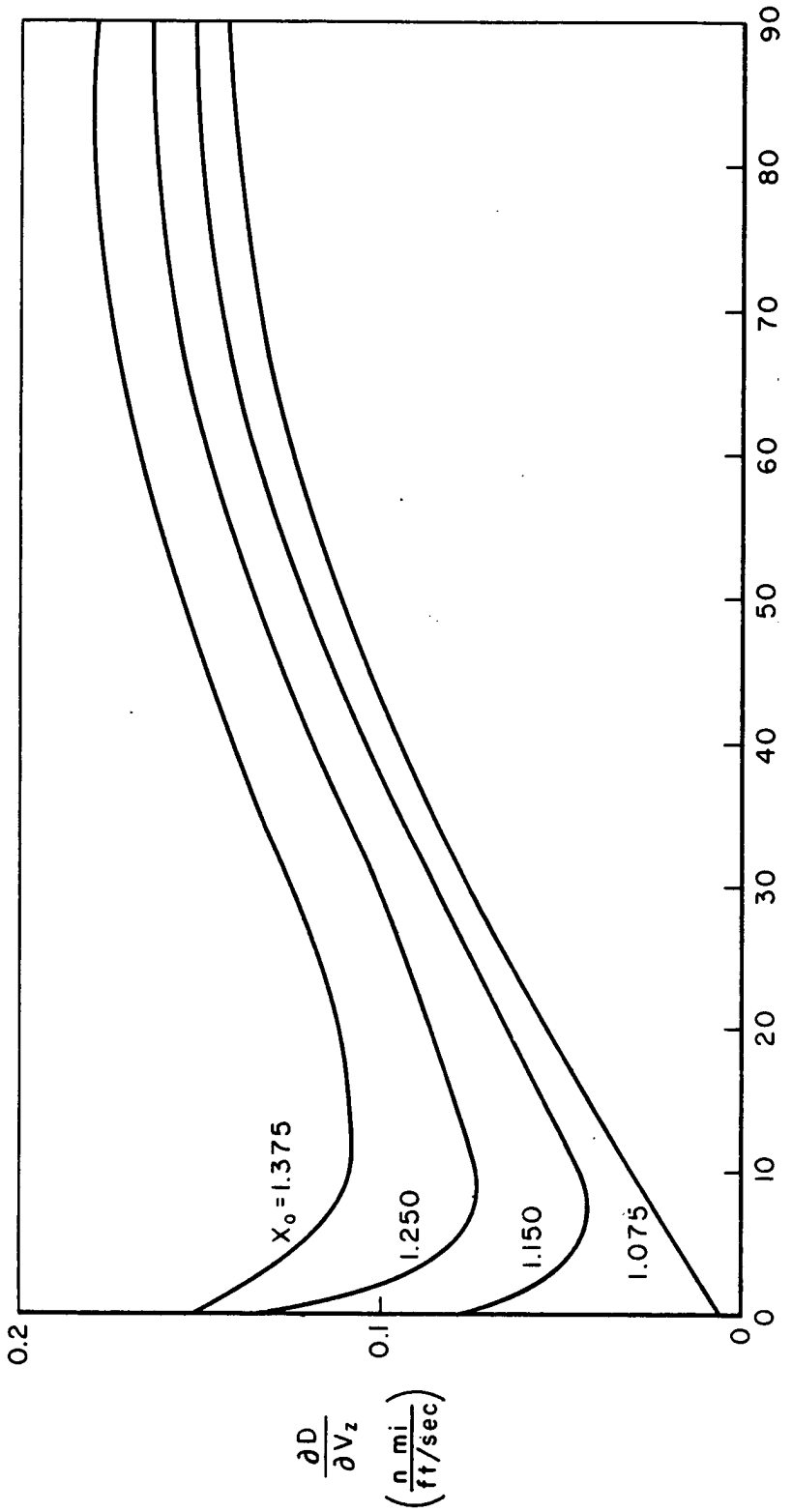

Fig. 14 — $\frac{\partial D}{\partial V_z}$ vs range angle

IV. DISCUSSION OF RESULTS

The velocity diagram developed in Sec. II, an example of which is shown in Figs. 5, 6, and 7, constitutes a very useful method for visualizing the effects of initial velocity and path direction on the subsequent motion of a vehicle which starts at a radial distance r_o from the center of the earth. On the basis of the position of the vehicle velocity vector, it is immediately possible to establish whether the subsequent path will impact on the earth, continue as a satellite, or escape the earth's gravitational field. In addition the various contours make it possible to determine the range of impact trajectories and the shape and orientation of resulting satellite orbits.

The diagram is also useful in determining the velocity change required to go from one path to another through a given initial point. In particular this method was used in Sec. III to determine the minimum velocity change required to go from a circular satellite orbit of radius x_o to impact at a range θ_1 from the initial point. The selection of this minimum velocity change has two advantages. First, it reduces the weight and space required in the vehicle for propulsion, and, second, it minimizes the resulting range dispersion of the impact point. Actually this minimum dispersion is dependent upon the assumption that the errors in the knowledge of satellite position and velocity are negligible at the time of velocity change; thus, any error in the resultant velocity is due to errors in the velocity change V_1. Owing to the geometry of the minimum configuration, the range error is most sensitive to errors in the magnitude of V_1, and for small attitude errors the range error is zero. This is a fortunate circumstance in that a precise control of the vehicle attitude is more difficult than a precise

control of the magnitude of the applied impulse.

However, as a hedge against the possibility that satellite tracking does have appreciable errors, the complete expressions for range and deflection errors are shown in an Appendix, taking into account satellite position and velocity errors as well as errors in the velocity change.

An examination of Figs. 10 through 13 shows that, for a given value of x_o, the larger the value of the minimum velocity change, V_1, the shorter the range to impact, θ_1. Also, the value of the dispersion derivative $\partial R/\partial V_1$ increases with increasing range - as would be expected from an examination of Fig. 5, since the spacing between contours of constant range is greater in the region of shorter impact range. Thus it is seen that from the point of view of range accuracy it is desirable to have a large value of V_1 and thus a short range to impact; while from the point of view of weight and space requirements for the propulsion system it is desirable to have a small value of V_1 with the correspondingly greater range to impact. Optimization of these two effects requires additional and as yet unavailable information as to the design and performance of the propulsion and attitude control systems of the vehicle.

A further examination of Figs. 10 through 13 shows that for a given value of the velocity change, V_1, the resulting range dispersion is less for smaller values of the initial radial distance, x_o. Also, the range to impact decreases with x_o for a given value of V_1. Thus from the point of view of range accuracy, it is desirable to make the altitude of the initial point as low as possible. However, it is necessary that the orbital altitude be large enough so that aerodynamic drag does not affect the path appreciably. This condition would probably mean that the minimum orbital altitude should

be not less than 300 mi.

While the dispersion derivatives for deflection errors shown in Fig. 14 are smaller in magnitude than those for range dispersion, it should be noted that errors in V_z arise when V_1 does not lie in the trajectory plane. As indicated previously, the problem of controlling the direction of V_1 is probably more difficult than determining its magnitude; thus the resulting deflection error may be of the same order as the range error.

In order to refine the preliminary results presented in this report it will be necessary to consider the effects of earth rotation in producing motion of the desired impact point relative to the trajectory plane and the deviation of the trajectory due to atmospheric re-entry, as well as possible re-entry heating limitations. Also the determination of a realistic value of the circular probable error of the vehicle will depend upon more detailed evaluation of the capabilities of the satellite tracking and prediction system as well as the vehicle propulsion and attitude control system.

V. CONCLUSIONS

As a result of the foregoing analysis and discussion, the following conclusions can be stated.

- The velocity diagram developed here constitutes a convenient tool for determining the behavior of a satellite vehicle subsequent to the application of an additional velocity impulse. The minimum required value of the velocity change and its direction of application for a given range to impact are determined for several values of initial altitude.
- The use of the minimum value of the velocity change results in a minimum value for the resulting range dispersion at impact.

Appendix

DISPERSION OF A RECOVERABLE SATELLITE

In the body of this report the dispersion derivatives were evaluated for the recoverable satellite application under the assumption that the satellite orbit was known with sufficient accuracy to insure that there was no error in the knowledge of the vehicle position and velocity at the time the recovery process was initiated. The present analysis gives a more general treatment of the dispersion problem, taking into account errors in the position and velocity at the time of initiation as well as errors in the magnitude and direction of the velocity change.

The geometry of this problem is shown in Fig. 15, where V_s and γ_s are the satellite velocity and path direction at the time of initiation and the other variables are the same as those in Fig. 8. In general the expression for the range error can be given as follows:

$$\Delta R = \frac{\partial R}{\partial \theta_o} \Delta\theta_o + \frac{\partial R}{\partial r_o} \Delta r_o + \frac{\partial R}{\partial V_o} \Delta V_o + \frac{\partial R}{\partial V_n} \Delta V_n \qquad (48)$$

where $\frac{\partial R}{\partial V_o}$ and $\frac{\partial R}{\partial V_n}$ are defined in Eqs. (39) and (40); while Ref. 3 gives the following

$$\frac{\partial R}{\partial \theta_o} = R_o \qquad (49)$$

$$\frac{\partial R}{\partial r_o} = \frac{\sin \frac{\theta_1}{2} \left[2x_o \cos\gamma_o - \cos(\theta_1 + \gamma_o) \right]}{x_o \cos\gamma_o \cos \frac{\theta_1}{2} - \cos\left(\frac{\theta_1}{2} + \gamma_o\right)} \qquad (50)$$

where $\Delta\theta_o$ is the range-angle error at the initial point.

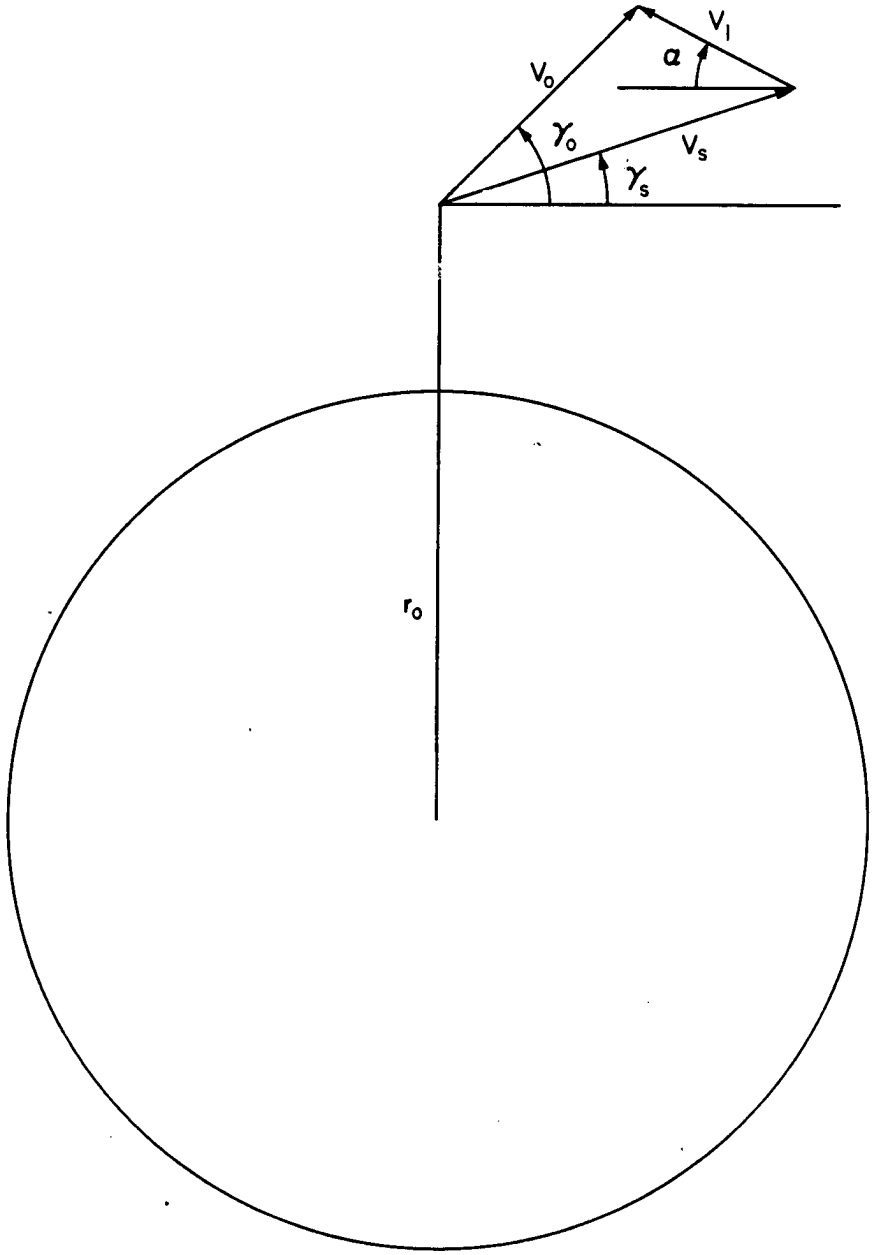

Fig. 15 — Dispersion geometry

From Fig. 15, it can be shown that

$$\Delta V_o = - \Delta V_1 \cos (\alpha + \gamma_o) + V_1 \Delta\alpha \sin (\alpha + \gamma_o) + \Delta V_s \cos (\gamma_o - \gamma_s) + V_s \Delta\gamma_s \sin (\gamma_o - \gamma_s) \quad (51)$$

$$\Delta V_N = V_o \Delta\gamma_o = \Delta V_1 \sin (\alpha + \gamma_o) + V_1 \Delta\alpha \cos (\alpha + \gamma_o) - \Delta V_s \sin (\gamma_o - \gamma_s) + V_s \Delta\gamma_s \cos (\gamma_o - \gamma_s) \quad (52)$$

In these two equations, it should be noted that the quantity $\Delta\alpha$ also includes the effect of the error in position, $\Delta\theta_o$, since α is measured from an incorrect horizontal reference.

Thus

$$\Delta\alpha = \frac{\Delta V_{ln}}{V_1} + \Delta\theta_o \quad (53)$$

Combination of Eqs. (48), (51), (52), and (53) gives the range error as

$$\Delta R = \left(\frac{\partial R}{\partial \theta_o} + V_1 \frac{\partial R}{\partial V_{ln}}\right) \Delta\theta_o + \frac{\partial R}{\partial r_o} \Delta r_o + \frac{\partial R}{\partial V_s} \Delta V_s + \frac{\partial R}{\partial V_{sn}} \Delta V_{sn} + \frac{\partial R}{\partial V_1} \Delta V_1 + \frac{\partial R}{\partial V_{ln}} \Delta V_{ln} \quad (54)$$

where

$$\frac{\partial R}{\partial V_1} = - \frac{\partial R}{\partial V_o} \cos (\alpha + \gamma_o) + \frac{\partial R}{\partial V_n} \sin (\alpha + \gamma_o) \quad (55)$$

$$\frac{\partial R}{\partial V_{ln}} = \frac{\partial R}{\partial V_o} \sin (\alpha + \gamma_o) + \frac{\partial R}{\partial V_n} \cos (\alpha + \gamma_o) \quad (56)$$

$$\frac{\partial R}{\partial V_s} = \frac{\partial R}{\partial V_o} \cos (\gamma_o - \gamma_s) - \frac{\partial R}{\partial V_n} \sin (\gamma_o - \gamma_s) \quad (57)$$

$$\frac{\partial R}{\partial V_{sn}} = \frac{\partial R}{\partial V_o} \sin (\gamma_o - \gamma_s) + \frac{\partial R}{\partial V_n} \cos (\gamma_o - \gamma_s) \qquad (58)$$

Equation (54) represents the complete expression for the error in range. In the body of the report a special case of this relation was used in which it was assumed that

$$\Delta\theta_o = \Delta r_o = \Delta V_s = \Delta V_{sn} = 0 \qquad (59)$$

In addition, values of V_1 and α were selected such that

$$\frac{\partial R}{\partial V_{1n}} = 0 \qquad (60)$$

Under these conditions Eq. (54) reduces to Eq. (46).

It is entirely possible that the assumption of perfect satellite tracking data may be incorrect, and in particular the error $\Delta\theta_o$ of the initial point may be quite significant. An examination of Eq. (54) shows that the effect of this error can be minimized by setting.

$$\frac{\partial R}{\partial \theta_o} = - V_1 \frac{\partial R}{\partial V_{1n}} \qquad (61)$$

which becomes

$$\frac{\partial R}{\partial V_{1n}} = - \frac{R_o}{V_1} \qquad (62)$$

This optimum condition results from a compensation of errors in initial position and the associated errors in the resultant velocity direction. In order to achieve this condition, the velocity change would have to be directed upward and to the rear ($0 < \alpha < \frac{\pi}{2}$). The decision as to whether to design for the optimum specified by Eq. (60) or for that given by Eq. (62) depends upon the relative capabilities of the satellite tracking

system and the vehicle propulsion and attitude control system, in the final analysis the true optimum for V_1 and α will probably lie between these two conditions.

The corresponding complete expression for the deflection dispersion from Ref. 3 is expressed as

$$\Delta D = \frac{\partial D}{\partial V_{sz}} \Delta V_{sz} + \frac{\partial D}{\partial V_{lz}} \Delta V_{lz} + \frac{\partial D}{\partial z} \Delta z \tag{63}$$

where

$$\frac{\partial D}{\partial V_{sz}} = \frac{\partial D}{\partial V_{lz}} = \frac{R_o \sin \theta_1}{V_o \cos \gamma_o} \tag{64}$$

$$\frac{\partial D}{\partial z} = \frac{R_o \cos (\theta_1 + \gamma_o)}{r_o \cos \gamma_o} \tag{65}$$

Equation (62) reduces to Eq. (47) for the conditions

$$\Delta z = 0 \tag{66}$$

$$\Delta V_{sz} + \Delta V_{lz} = \Delta V_z \tag{67}$$

It is seen from Eq. (65) that the effect of lateral position errors can be reduced to zero by making the sum of θ_1 and γ_o equal to 90 deg. However, it does not appear that the effect of this error is sufficient to warrant an optimization on this basis.

REFERENCES

1. Huntzicker, J. H. and H. A. Lieske, Physical Recovery of Satellite Payloads - A Preliminary Investigation (U), The RAND Corporation, Research Memorandum RM-1811, 26 June 1956 (Secret).

2. Frick, R. H., Graphical Determination of Ballistic Trajectories - Through Outer Space with Compass and Straightedge, The RAND Corporation, Research Memorandum RM-1641, 24 February 1956.

3. Frick, R. H., Ballistic Missile Accuracy at Reduced Range (U), The RAND Corporation, Research Memorandum RM-1712, 8 June 1956 (Secret).